Article

SOURCE DATA | TRANSPARENT PROCESS | OPEN ACCESS

EMBO reports

Tmem117 in AVP neurons regulates the counterregulatory response to hypoglycemia

Sevasti Gaspari, Gwenaël Labouèbe, Alexandre Picard, Xavier Berney, Ana Rodriguez Sanchez-Archidona & Bernard Thorens*

Abstract

The counterregulatory response to hypoglycemia (CRR), which ensures a sufficient glucose supply to the brain, is an essential survival function. It is orchestrated by incompletely characterized glucose-sensing neurons, which trigger a coordinated autonomous and hormonal response that restores normoglycemia. Here, we investigate the role of hypothalamic *Tmem117*, identified in a genetic screen as a regulator of CRR. We show that *Tmem117* is expressed in vasopressin magnocellular neurons of the hypothalamus. *Tmem117* inactivation in these neurons increases hypoglycemia-induced vasopressin secretion leading to higher glucagon secretion in male mice, and this effect is estrus cycle phase dependent in female mice. *Ex vivo* electrophysiological analysis, *in situ* hybridization, and *in vivo* calcium imaging reveal that *Tmem117* inactivation does not affect the glucose-sensing properties of vasopressin neurons but increases ER stress, ROS production, and intracellular calcium levels accompanied by increased vasopressin production and secretion. Thus, *Tmem117* in vasopressin neurons is a physiological regulator of glucagon secretion, which highlights the role of these neurons in the coordinated response to hypoglycemia.

Keywords counterregulation; glucagon; hypoglycemia; *Tmem117*; vasopressin
Subject Categories Metabolism; Neuroscience
DOI 10.15252/embr.202357344 | Received 14 April 2023 | Revised 21 May 2023 | Accepted 31 May 2023 | Published online 14 June 2023
EMBO Reports (2023) 24: e57344

Introduction

The brain relies almost exclusively on glucose for metabolic energy production. Therefore, maintaining blood glucose levels no lower than ~5 mM is essential for survival (Marty *et al*, 2007). When glycemic levels drop below this threshold, a brain-orchestrated neuroendocrine reflex triggers a counterregulatory response (CRR). This is characterized by the secretion of multiple hormones that act on peripheral target organs to stimulate endogenous glucose production, suppress insulin secretion, and minimize glucose utilization to restore normoglycemia (Tesfaye & Seaquist, 2010). A key aspect of the CRR is the induction of glucagon (GCG) secretion from pancreatic alpha cells, which triggers enhanced glucose production from the liver (Ramnanan *et al*, 2011; Thorens, 2022). Patients with type 1 or advanced type 2 diabetes display loss of hypoglycemia-induced GCG secretion (Cryer, 2012; Siafarikas *et al*, 2012; Bisgaard Bengtsen & Møller, 2021), but the underlying mechanism is poorly understood. In addition to deregulated alpha cell autonomous and intraislet paracrine interactions (Gaisano *et al*, 2012), evidence suggests that defects in the central nervous system (CNS) control of GCG secretion contribute to this blunted response (Beall *et al*, 2012; Stanley *et al*, 2019).

In the CNS, changes in glucose concentrations are detected by neurons located in several regions but have been studied most extensively in the hypothalamus and brainstem. Several hypothalamic areas are equipped with glucose-sensing neurons, including the ventromedial (VMH), dorsomedial (DMH), lateral, arcuate (ARC), paraventricular (PVN), and supraoptic (SON) nuclei (Stanley *et al*, 2019). Glucose responsive neurons are activated by either a rise (glucose excited/GE neurons) or a fall (glucose inhibited/GI neurons) in glucose levels. The response to hypoglycemia involves activation by GI neurons of both the parasympathetic and sympathetic branches of the autonomic nervous system, which stimulate GCG secretion and hepatic glucose production, the activation of the hypothalamus–pituitary–adrenal (HPA) axis to stimulate epinephrine and glucocorticoid secretion (Tesfaye & Seaquist, 2010), and the activation of hypothalamic vasopressin (AVP) neurons to stimulate GCG secretion through the actions of AVP on pancreatic alpha cell AVP V1b receptors (Gao *et al*, 1992; Yibchok-anun *et al*, 2004; Kim *et al*, 2021).

Multiple studies have provided evidence in support for the role of hypothalamic and brainstem glucose sensing neurons in CRR. For instance, cell-specific activation of VMH neuronal subpopulations expressing glucokinase (Gck) (Meek *et al*, 2016) or steroidogenic factor 1 (Sf1) (Stanley *et al*, 2016) increases GCG secretion and glycemia, while their inhibition blocks CRR. Interestingly, genetic inactivation of *Gck* in Sf1 neurons impairs GCG secretion in a sex-dependent manner (Steinbusch *et al*, 2016). Glucose responsive neurons located in other nuclei have also been shown to control GCG secretion. This is the case of cholecystokinin-expressing neurons of the parabrachial nucleus that control VMH neurons (Garfield *et al*, 2014), of fibroblast growth factor 15-expressing neurons of the DMH (Picard *et al*, 2016, 2021), and of Glut2 GI neurons of the

Center for Integrative Genomics, University of Lausanne, Lausanne, Switzerland
*Corresponding author. Tel: +41 21 2692 3981; Fax: +41 21 692 3985; E-mail: bernard.thorens@unil.ch

nucleus tractus solitarius, which activate vagal nerve firing to stimulate GCG secretion (Lamy *et al*, 2014).

To identify in an unbiased manner novel hypothalamic regulators of CRR induced by insulin-induced hypoglycemia, we performed a genetic screen using a panel of recombinant inbred BXD mouse lines, derived from the cross of C57Bl/6 and DBA/2 mice (Peirce *et al*, 2004). This screen (Picard *et al*, 2022) led to the identification of *Agpat5*, encoding a lipid biosynthesis enzyme, and the characterization of its essential role in the activation by hypoglycemia of AgRP neurons and GCG secretion (Strembitska *et al*, 2022). We further identified *Tmem117*, located in a QTL on chromosome 15, as another candidate regulator of GCG secretion. *Tmem117* encodes an eight transmembrane-containing membrane protein (Bürgi *et al*, 2016) that has been reported to negatively control ER stress and ROS production (Tamaki *et al*, 2017).

Here, we show that *Tmem117* is expressed in AVP magnocellular neurons, that AVP neurons are in large part GI neurons, and that hypoglycemia induces copeptin (CPP; an AVP surrogate) and GCG secretion. Genetic inactivation of *Tmem117* in AVP neurons increases, in a sex-dependent manner, hypoglycemia-induced CPP and GCG secretion. *Tmem117* inactivation does not affect the glucose sensing properties of AVP neurons but induces ER stress and increases intracellular ROS and Ca^{2+} levels as well as AVP mRNA expression.

Results

Tmem117 is expressed in AVP magnocellular neurons

A genetic screen of a panel of 36 recombinant inbred BXD mice for hypoglycemia-induced GCG secretion identified a clinical quantitative trait locus (cQTL) on chromosome 8 and one on chromosome 15 (Picard *et al*, 2022). The candidate gene on chromosome 8 encodes the lipid-modifying enzyme Agpat5, which is required for hypoglycemia sensing by AgRP neurons, vagal nerve activation, and GCG secretion (Strembitska *et al*, 2022). On chromosome 15, two genes showed strong negative correlation with the GCG trait, *Irak4* and *Tmem117* (Fig EV1A–D). The role of *Irak4* in controlling hypothalamic Il-1β signaling and GCG secretion has been reported (Picard *et al*, 2022). Here, we performed an expression QTL analysis (eQTL) for the level of *Tmem117* mRNA in the hypothalamus of the BXD mouse lines. We identified an eQTL on chromosome 15 at the same position of the cQTL (Fig EV1E). Thus, indicating that this genomic locus controls both GCG secretion and *Tmem117* expression.

To establish the sites of *Tmem117* expression in the hypothalamus we performed immunofluorescence microscopy analysis. We found strong immunolabeling for Tmem117 in the SON and PVN (Fig 1A) and in the posterior pituitary (Fig 1B). The specificity of the immunostaining was confirmed by the lack of signal in brains of mice with *Tmem117* gene inactivation in AVP neurons (*Tmem117*$^{fl/fl}$;*AVP-IRES-Cre-D*$^{tg/+}$ mice) (Fig 1C and D). Costaining for neuropeptides revealed that *Tmem117* was expressed in AVP magnocellular cells (Fig 1E–G). Quantification in three mice and two consecutive hypothalamic sections for each mouse (bregma −0.7 and −0.8) showed that ~90% of AVP neurons in the PVN and ~97% in the SON were Tmem117 positive (Fig 1H and I). Super-resolution microscopy revealed a punctuated intracellular distribution of Tmem117, which colocalized in part with AVP granules in both the soma and axons of magnocellular neurons (Fig 1J).

Tmem117 inactivation in AVP neurons increases insulin-induced copeptin and glucagon secretion

To inactivate *Tmem117* specifically in AVP neurons, we generated *Tmem117*^{fl} mice that allowed Cre-dependent excision of exon 3, which encodes the third transmembrane domain (amino acids 93–136) of the predicted structure of Tmem117 (Jumper *et al*, 2021; Varadi *et al*, 2022) (Fig EV2A and B). To induce *Tmem117*^{fl} recombination in AVP neurons, we used a viral-mediated approach for expression of Cre recombinase. This was preferred over the use of *AVP-IRES-Cre-D*$^{tg/+}$ mice because these display reduced endogenous AVP levels (Cheng *et al*, 2019). We, thus, constructed an AAV plasmid containing the full-length AVP promoter placed upstream of a codon-improved Cre recombinase (iCre) sequence (Ponzio *et al*, 2012) (Fig EV2C). The resulting plasmid was packaged in serotype 6 adeno-associated viruses (AAV6-AVP-iCre), which infect magnocellular neurons with high efficacy (Ponzio *et al*, 2012) and have a high retrograde transport capacity (Salegio *et al*, 2013). Injection of AAV6-AVP-iCre in the posterior pituitary of adult *Tmem117*$^{fl/fl}$ mice triggered efficient recombination in the PVN and SON as detected by PCR analysis of genomic DNA (Fig EV2D) and by the expression of tdTomato when the AAV6-AVP-iCre was injected in the posterior pituitary of *Rosa26*^{tdTomato} mice (Fig EV2E).

To assess the role of *Tmem117* in GCG secretion, *Tmem117*$^{fl/fl}$ and *Tmem117*$^{+/+}$ mice were injected with the AAV6-AVP-iCre in the posterior pituitary to generate AVP^{TM117KO} and AVP^{TM117WT} mice, respectively (Fig 2A). Two weeks later, the mice received an intraperitoneal (i.p.) injection of saline and blood was collected 1 h later for plasma CPP and GCG measurements. The same experiment was repeated 1 week later with injection of insulin instead of saline to

Figure 1. *Tmem117* is expressed in AVP magnocellular neurons.

Immunofluorescence microscopy detection of Tmem117 in the mouse hypothalamus and pituitary.

A, B Positive immunostaining was observed in the PVN, the SON, and the posterior pituitary.

C, D No immunostaining was detected in the hypothalamus and pituitary of mice with constitutive inactivation of *Tmem117* in AVP neurons.

E–G Costaining for Tmem117 and AVP in the (E) PVN, (F) SON, and (G) posterior pituitary.

H, I Quantification of AVP and Tmem117 double positive cells in the PVN and SON, respectively.

J Higher resolution depiction of an AVP and Tmem117 double positive neuron in the PVN captured with structured illumination microscopy. The white arrows highlight representative positions of signal colocalization.

Data information: 3V: third ventricle, AP: anterior pituitary, MZ: medial zone, opt: optic tract, PP: posterior pituitary, PVN: paraventricular nucleus, SCh: suprachiasmatic nucleus, SON: supraoptic nucleus. Scale bar = 100 μm for panels A–G, =10 μm for panel J.

Source data are available online for this figure.

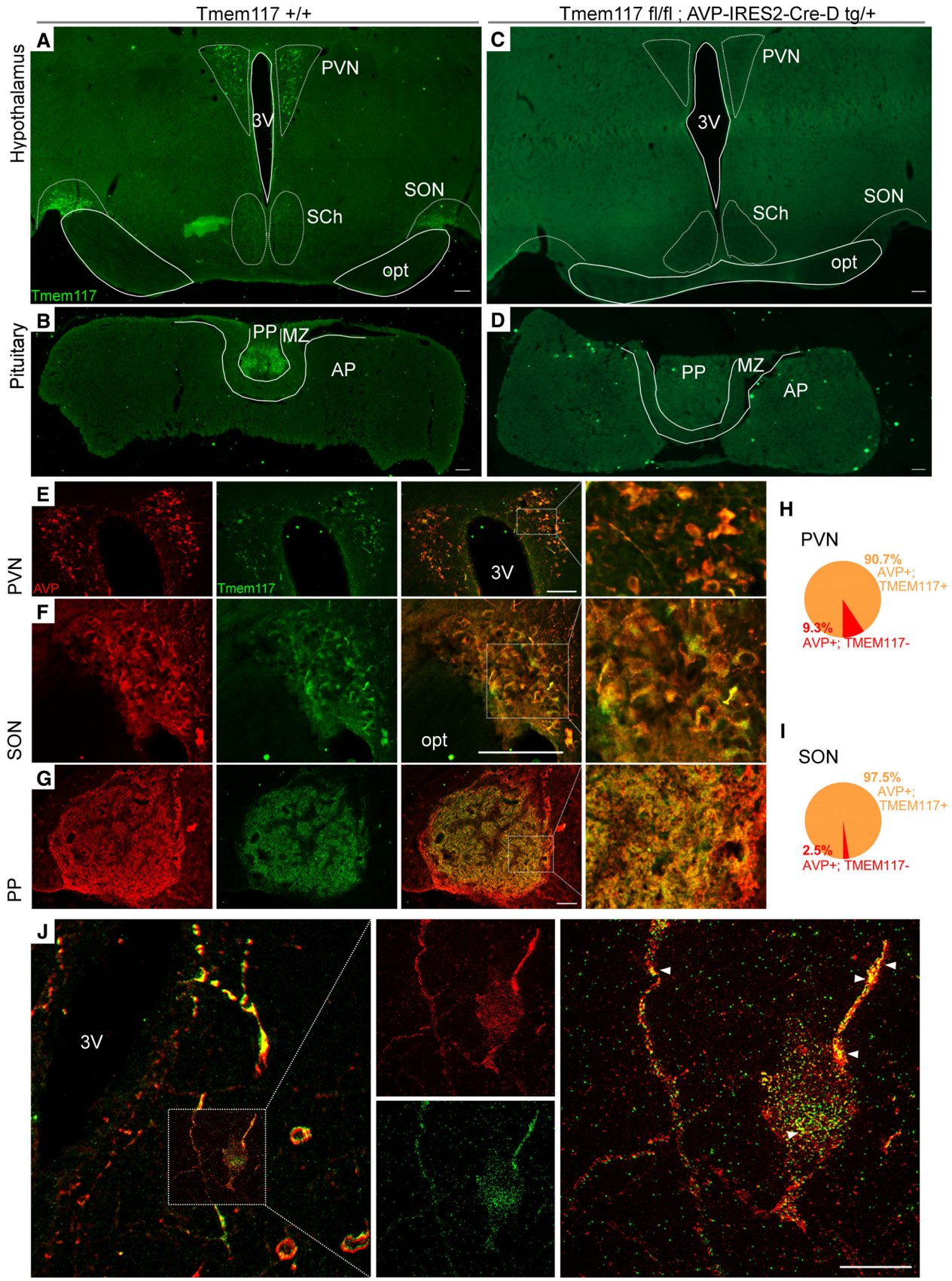
Tmem117 +/+
Tmem117 fl/fl ; AVP-IRES2-Cre-D tg/+
Hypothalamus
Pituitary
A
B
C
D
PVN
3V
SON
SCh
opt
Tmem117
PP
MZ
AP
E
F
G
PVN
SON
PP
AVP
Tmem117
H
PVN
90.7%
AVP+;
TMEM117+
9.3%
AVP+; TMEM117-
I
SON
97.5%
AVP+;
TMEM117+
2.5%
AVP+; TMEM117-
J

Figure 1.

induce hypoglycemia. Insulin induced the same hypoglycemic levels in AVP^{TM117WT} and AVP^{TM117KO} male mice (Fig 2B); CPP secretion was increased in both groups of mice, but significantly more in AVP^{TM117KO} mice than in AVP^{TM117WT} mice (Fig 2C); the same pattern was observed for the secretion of GCG (Fig 2D).

Female AVP^{TM117WT} mice and *AVP*^{TM117KO} mice were then tested in the same conditions. Insulin induced the same level of hypoglycemia (Fig 2E) and triggered comparable secretion of CPP and GCG in both groups of mice (Fig 2F and G). However, when the hormone levels were analyzed separately for each phase of the estrus cycle, we found that while the insulin-induced hypoglycemic levels were comparable across the estrus cycle between genotypes (Fig 2H), the level of secreted CPP and GCG were significantly higher in AVP^{TM117KO} mice as compared to AVP^{TM117WT} mice during the proestrus phase (Fig 2I and J).

Glucose responsiveness of SON AVP neurons is not affected by *Tmem117* inactivation

To assess whether AVP neurons were activated by insulin-induced hypoglycemia, C57Bl/6N male mice were injected with a saline solution or with insulin and their brains were collected 2 h later. Immunofluorescence microscopy analysis revealed that hypoglycemia (<3.9 mmol/l) robustly increased c-Fos expression in both PVN and SON (Fig 3A–E) with an approximately threefold increase in the number of c-Fos^{+} AVP neurons compared to the saline injected controls (Fig 3C and F). Furthermore, analysis of microdissected PVN and SON tissue 1 h after insulin injection revealed downregulation of *Tmem117* mRNA in the SON (Fig 3G–I).

To determine whether *Tmem117* inactivation would modify insulin-induced c-Fos expression in AVP neurons, we prepared AVP^{TM117KO} mice and AVP^{TM117WT} control mice by injection of AAV6-AVP-iCre in the posterior pituitary of *Tmem117*$^{fl/fl}$ and *Tmem117*$^{+/+}$ male mice (Fig 4A). Two weeks later, the mice were treated as described earlier for the C57Bl/6N. Induction of c-Fos expression in AVP neurons of the SON was comparable between the two mouse groups (Fig 4B and C).

To determine whether AVP neurons were sensitive to the decreased glucose availability and whether *Tmem117* would modify this sensitivity, we performed patch clamp recordings of AVP neurons in the presence of 2.5 and 0.1 mM glucose (Labouèbe *et al*, 2018). *Tmem117*$^{+/+}$ and *Tmem117*$^{fl/fl}$ adult male mice were coinjected in the SON with AAV6-AVP-iCre and an AAV8-DIO-mCherry to allow fluorescence visualization of the AVP neurons (Fig 4D). SON was preferred over PVN due to its homogeneous magnocellular AVP population. Direct injection was used instead of retrograde labeling by injection in the posterior pituitary due to its higher labeling efficiency. One to two weeks after surgery, we performed patch clamp analysis of AVP neurons. In brain slices of AVP^{TM117WT} mice, we found that approximately half of the recorded AVP neurons were activated by low glucose (GI neurons) and that the other half were glucose nonresponder (NR) neurons; no glucose excited (GE) neurons were observed (Fig 4E–H; black). When the same measurements were performed in cells with *Tmem117* gene inactivation, the proportion of GI and NR cells and their membrane potential responses were similar to that of AVP^{TM117WT} mice (Fig 4E–H; red). Thus, AVP neurons were in large part GI neurons and *Tmem117* inactivation did not alter their glucose responsiveness. Furthermore, exposure of AVP neurons to low glucose concentration decreased the membrane resistance of six of seven *AVP*^{TM117KO} GI cells and six of nine *AVP*^{TM117WT} GI cells (Fig 4I), with no effect in NR cells of both genotypes (Fig 4J), suggesting a cell autonomous response to hypoglycemia at least in a subpopulation of AVP GI neurons. However, given that the overall comparison did not reach statistical significance, this is just a suggestive observation.

Tmem117 inactivation increases ER stress, ROS production, intracellular Ca^{2+} levels, and AVP mRNA expression

Tmem117 has been identified in a siRNA screen of the HTC116 colon cancer cell line as a negative regulator of ER stress and ROS production (Tamaki *et al*, 2017). To verify its contribution to ER stress, we used the colon adenocarcinoma cell line SW480, which endogenously expresses *Tmem117*. SW480 cells were transfected with a siRNA targeting *Tmem117* or a siRNA control and 48 h later the cells were collected for RNA and protein extraction. A small reduction in *Tmem117* mRNA levels (log_2fold approximately −0.5) robustly increased expression of the ER stress markers *sXbp1* and *BiP* (Fig EV3A) and calnexin (Fig EV3B). *Tmem117* silencing in this cell line did not increase ROS production (Fig EV3C), but *Tmem117* overexpression significantly reduced ROS production (Fig EV3D). These data confirm a link between *Tmem117* expression and ER stress and ROS production in carcinoma cell lines.

To test whether inactivation of *Tmem117* in AVP magnocellular neurons *in vivo* would also affect ER stress and ROS production, we prepared *AVP*^{TM117KO} and *AVP*^{TM117WT} mice by injecting AAV6-

Figure 2. *Tmem117* inactivation in AVP neurons enhances hypoglycemia-induced copeptin and glucagon secretion.

A Experimental scheme. AAV6-AVP-iCre was injected in the posterior pituitary of *Tmem117*$^{fl/fl}$ (AVP^{TM117KO}) or *Tmem117*$^{+/+}$ (AVP^{TM117WT}) mice.
B Glycemia of male mice 1 h after saline (black) or insulin (red) i.p. injection (n = 15–16 mice per group).
C CPP plasma levels of male mice 1 h after saline or insulin injection (n = 13 mice per group; mean ± SEM for INS: WT 89 ± 5 vs. KO 121 ± 13 pg/ml).
D GCG plasma levels of male mice 1 h after saline or insulin injection (n = 15–16 mice per group; mean ± SEM for INS: WT 124 ± 19 vs. KO 186 ± 21 pg/ml).
E Glycemia of female mice 1 h after saline (black) or insulin (red) i.p. injection (n = 18–22 mice per group).
F CPP plasma levels of female mice 1 h after saline or insulin injection (n = 18–19 mice per group; mean ± SEM for INS: WT 78 ± 6 vs. KO 92 ± 8 pg/ml).
G GCG plasma levels of female mice 1 h after saline or insulin injection (n = 17–20 mice per group; mean ± SEM for INS: WT 242 ± 14 vs. KO 277 ± 18 pg/ml).
H–J Analysis of glycemic levels and of CPP and GCG secretion following insulin injection in female mice at each stage of the estrus cycle (n = 3–7 mice per group). (H) Glycemic levels. (I) CPP plasma levels. (J) GCG plasma levels.

Data information: d: day, di: diestrus, est: estrus, INS: insulin, met: metestrus, PP: posterior pituitary, pro: proestrus, SAL: saline. For panels B–G, bars correspond to the mean value per group. For panels H–J, lines correspond to the mean value per group and error bars represent ± SEM. B–G: two-way ANOVA RM with Bonferroni *post hoc* test; H–J: unpaired *t* test; *P < 0.05, **P < 0.01, ***P < 0.001.
Source data are available online for this figure.

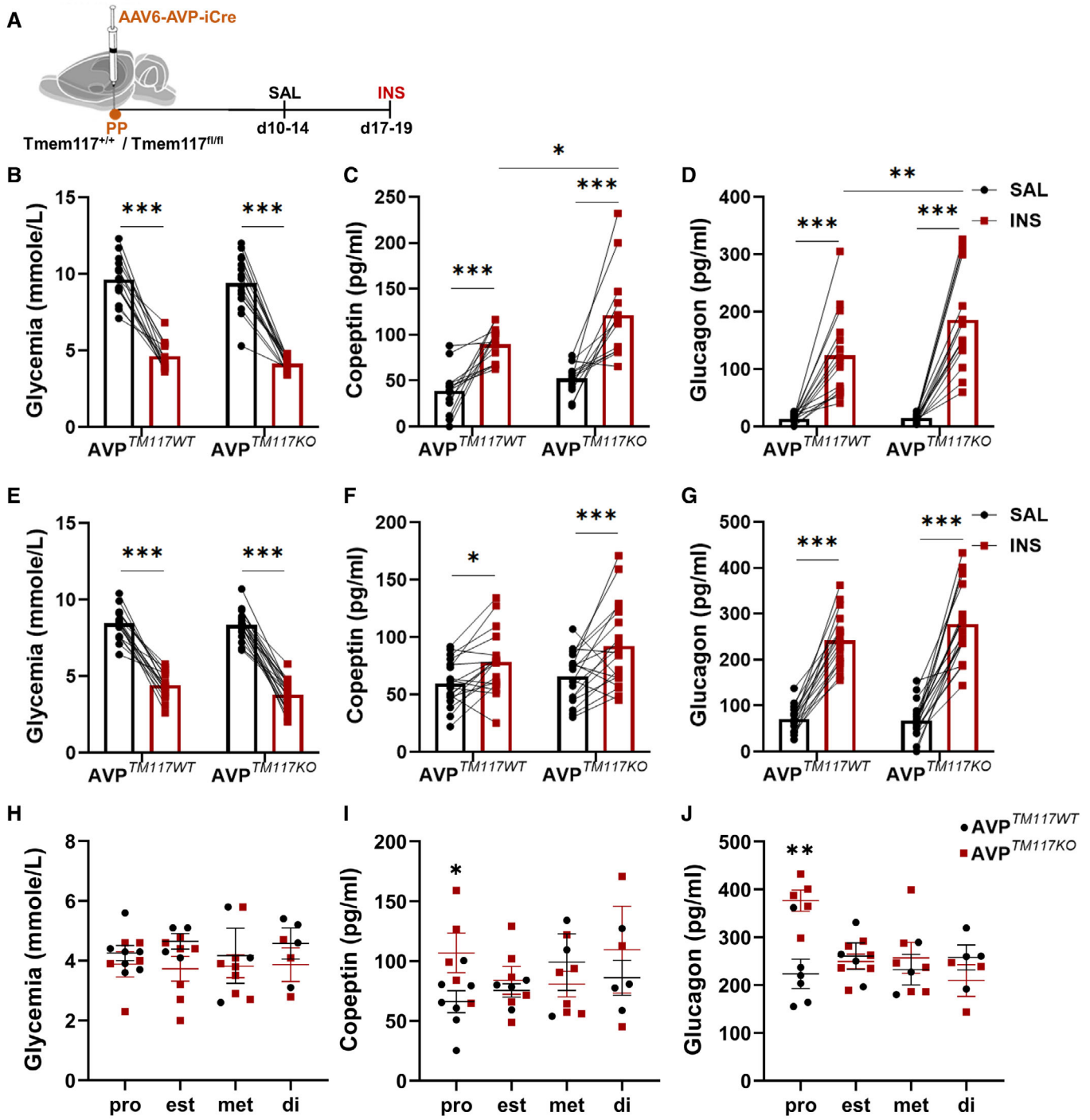

Figure 2.

AVP-iCre in the posterior pituitary of *Tmem117*$^{fl/fl}$ and *Tmem117*$^{+/+}$ mice. Two weeks later, we collected their brains and measured the level of *Bip* mRNA by *in situ* hybridization (RNAScope). Quantitative analysis at the single-cell level revealed higher expression of *Bip* mRNA in AVP neurons of *AVP*^{TM117KO} mice as compared to those of *AVP*^{TM117WT} mice; non-AVP cells in the SON showed no difference in *Bip* mRNA expression between the two groups of mice (Fig 5A–C). Furthermore, we found markedly elevated levels of AVP mRNA in AVP^{TM117KO} mice as compared to control mice (Fig 5C and D). AVP transcription has been reported to be induced by ROS (St-Louis *et al*, 2012, 2014). We, thus, assessed the ROS levels in the SON by injecting i.p. the fluorescent ROS indicator dihydroethidium (DHE) in *AVP*^{TM117KO} and *AVP*^{TM117WT} mice 24 h before tissue collection (Fig 5E). Quantification of the DHE fluorescence intensity revealed higher ROS production in the SON of *AVP*^{TM117KO} mice (Fig 5F and G).

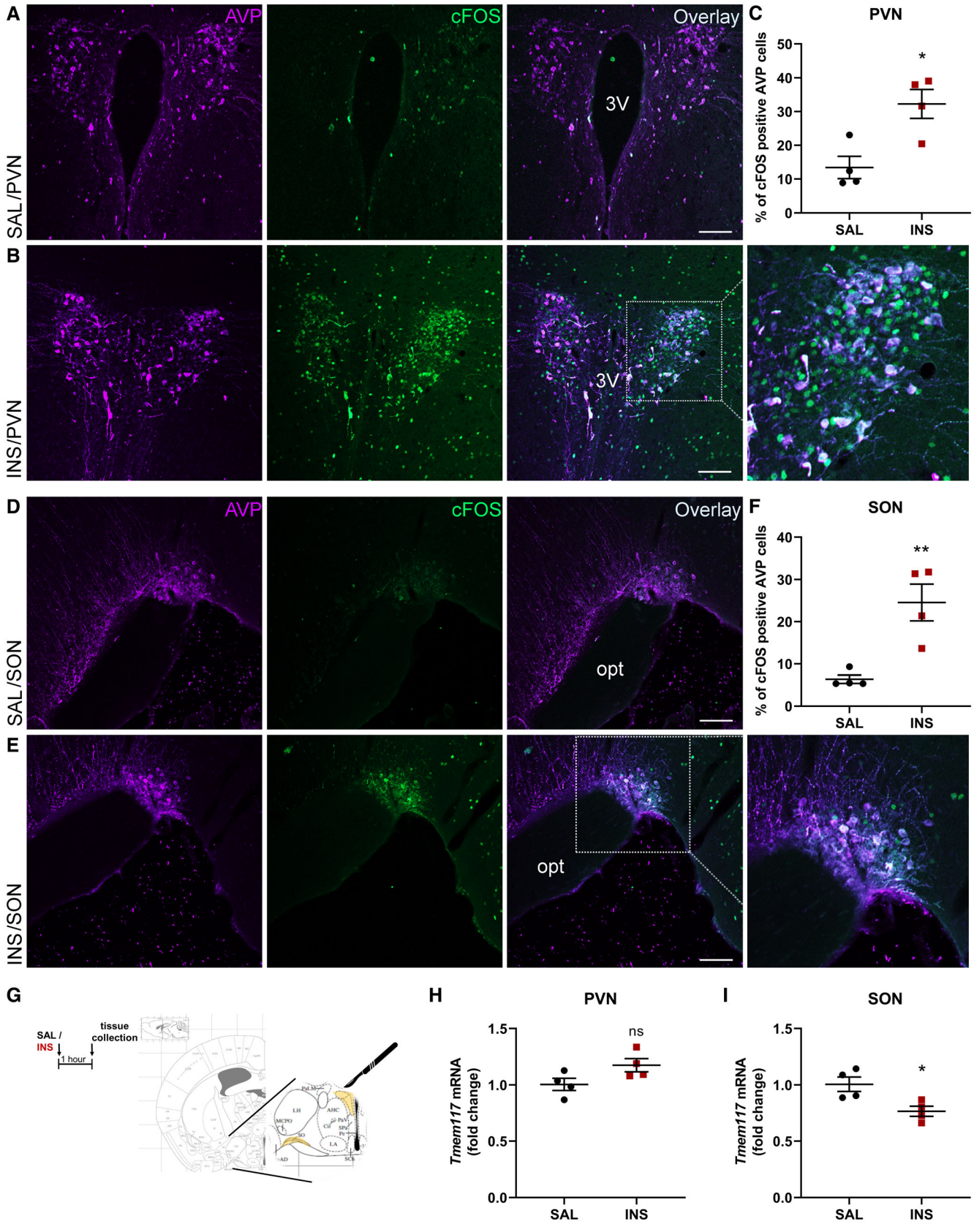

Figure 3.

Figure 3. Insulin-induced hypoglycemia triggers activation of AVP magnocellular neurons and reduces *Tmem117* mRNA levels in the SON.

A–F C57BL6/N male mice were injected i.p. with saline or insulin and c-Fos expression (green) in AVP (magenta) neurons was quantitated by immunofluorescence microscopy 2 h later. (A) c-Fos expression in the PVN after saline injection. (B) c-Fos expression in the PVN after insulin injection. (C) Quantitation of c-Fos-positive AVP cells in the PVN after saline and insulin injections (n = 4 mice per group). (D) c-Fos expression in the SON after saline injection. (E) c-Fos expression in the SON after insulin injection. (F) Quantitation of c-Fos-positive AVP cells in the SON after saline and insulin injections (n = 4 mice per group).

G–I C57Bl/6N male mice were injected i.p. with saline or insulin and brain tissue was collected 1 h later. PVN and SON were microdissected for quantification of *Tmem117* mRNA levels by RT-PCR. (H) *Tmem117* mRNA levels in the PVN (n = 4 mice per group). (I)*Tmem117* mRNA levels in the SON (n = 4 mice per group).

Data information: 3V: third ventricle, AVP: vasopressin, INS: insulin, opt: optic tract, PVN: paraventricular nucleus, SAL: saline, SON: supraoptic nucleus. Scale bar = 100 μm. Lines correspond to the mean value per group and error bars represent ± SEM. Unpaired t test; ns: $P > 0.05$, *$P < 0.05$, **$P < 0.01$.
Source data are available online for this figure.

Both ER stress and ROS can increase intracellular Ca^{2+} concentrations (Giorgi *et al*, 2018), which would enhance neurosecretion. We, thus, measured the intracellular Ca^{2+} levels in AVP neuronal terminals at the posterior pituitary, the site of AVP exocytosis, by *in vivo* fiber photometry. $AVP^{TM117KO}$ and $AVP^{TM117WT}$ mice were prepared by coinjection of the AAV6-AVP-iCre virus and an AAV9-hsyn-FLEX-jGCaMP7 in the posterior pituitary of $Tmem117^{fl/fl}$ and $Tmem117^{+/+}$ mice. During the same surgery an optic fiber cannula was implanted in the posterior pituitary for fluorescence monitoring (Fig 5H). Two weeks later, the baseline jGCaMP7 fluorescence signal was recorded in both control and knockout mice. This showed that inactivation of *Tmem117* induced a markedly higher baseline Ca^{2+} signal (Fig 5I). We then performed Ca^{2+} recordings after insulin-induced hypoglycemia. The first measures were performed at days 14–16 after viral injection. A second session of recording was performed over days 19–24 in $AVP^{TM117WT}$ mice injected with saline and these data were used as control for the first set of experiments. For both sessions, the Ca^{2+} signal was recorded during a 30-min baseline period and for 1 h following i.p. insulin or saline injections (Fig 5J). Each signal was normalized to the mean intensity of the baseline (corresponding to the last 10 min preceding the i.p. injection) and the area under the curve (AUC) was quantified for the mean trace of each group over 10-min period (Fig 5K). In $AVP^{TM117WT}$ mice, insulin injection increased the Ca^{2+} signal as compared to saline injection, a difference that became significant 20 min after the injection. In $AVP^{TM117KO}$ mice, insulin induced a significantly higher Ca^{2+} signal than in $AVP^{TM117WT}$ mice already 10 min after injection (Fig 5J and K). The correct placement of the optic fiber (Fig 5L) was assessed at the end of each experiment and the expression of jGCaMP7 in AVP magnocellular terminals was verified by fluorescence microscopy (Fig 5M).

Together, the above experiments indicate that *Tmem117* inactivation in AVP magnocellular neurons triggered ER stress, increased ROS production, intracellular Ca^{2+} levels, and AVP mRNA levels.

Tmem117 inactivation progressively triggers cell death

Permanently elevated ER stress and increased levels of intracellular ROS and Ca^{2+} may trigger cell death (Zhivotovsky & Orrenius, 2011; Iurlaro & Muñoz-Pinedo, 2016; Giorgi *et al*, 2018). Therefore, we investigated the fate of AVP neurons 1 month after *Tmem117* inactivation in $Tmem117^{fl/fl}$ mice coinjected in the SON with AAV6-AVP-iCre and AAV9-hsyn-DIO-EGFP ($AVPT^{M117KO}$ mice). Two groups of control mice were prepared. One consisted of $Tmem117^{+/+}$ mice injected with both viruses ($AVP^{TM117WT}$ mice); these allowed to assess by immunofluorescence microscopy the total number of $Tmem117^{+}$ cells and the total number of infected, EGFP-expressing cells. The second group consisted of $Tmem117^{fl/fl}$ mice injected only with AAV9-hsyn-DIO-EGFP ($AVP^{TM117FL}$ mice), which were used as control for the effect of the genotype on the total number of $Tmem117^{+}$ cells in the SON (Fig EV4A). Fluorescence microscopy images of EGFP and Tmem117 and of DAPI staining for the three groups are presented in Fig EV4B.

Quantitative analysis of the immunofluorescence data showed that the total number of $Tmem117^{+}$ cells was the same in the two control groups but was reduced by ≥ 50% in $AVP^{TM117KO}$ mice as compared to the control mice (Fig EV4C). When considering only the $EGFP^{+}$ and $Tmem117^{+}$ double-labeled cells, the reduction was even more striking, reaching ~75% (Fig EV4D), indicating that most

Figure 4. Glucose responsiveness of *Tmem117* KO AVP neurons.

A Experimental scheme. AAV6-AVP-iCre was injected in the posterior pituitary of $Tmem117^{fl/fl}$ ($AVP^{TM117KO}$) or $Tmem117^{+/+}$ ($AVP^{TM117WT}$) mice.
B c-Fos expression in the SON.
C Quantitation of c-Fos-positive AVP cells in the SON after saline and insulin injections (n = 4–5 mice per group).
D Experimental scheme. AAV6-AVP-iCre was coinjected with AAV8-DIO-mcherry in the SON of $Tmem117^{fl/fl}$ ($AVP^{TM117KO}$) or $Tmem117^{+/+}$ ($AVP^{TM117WT}$) mice.
E Proportion of GI and NR AVP neurons in the SON (n = 16–18 cells per group).
F Representative traces of GI and NR AVP neurons in each group.
G Membrane potential was increased comparably in response to 0.1 mM glucose in both groups (n = 7–9 cells per group).
H No change in membrane potential in NR neurons of both genotypes (n = 9 cells per group).
I Membrane resistance was decreased in six of nine $AVP^{TM117WT}$ and six of seven $AVP^{TM117KO}$ cells in response to 0.1 mM glucose (n = 7–9 cells per group).
J Membrane resistance in NR neurons was stable for both genotypes (n = 9 cells per group).

Data information: AVP: vasopressin, d: day, GI: glucose inhibited, INS: insulin, NR: nonresponding, opt: optic tract, SAL: saline, w: week. Scale bar = 100 μm. Lines correspond to the mean value per group and error bars represent ± SEM. C: Two-way ANOVA with Tukey's *post hoc* test; E: Fisher's exact test; G–J: paired t test for all graphs except Δ membrane potential (unpaired); ns $P > 0.05$, *$P < 0.05$, ***$P > 0.001$.
Source data are available online for this figure.

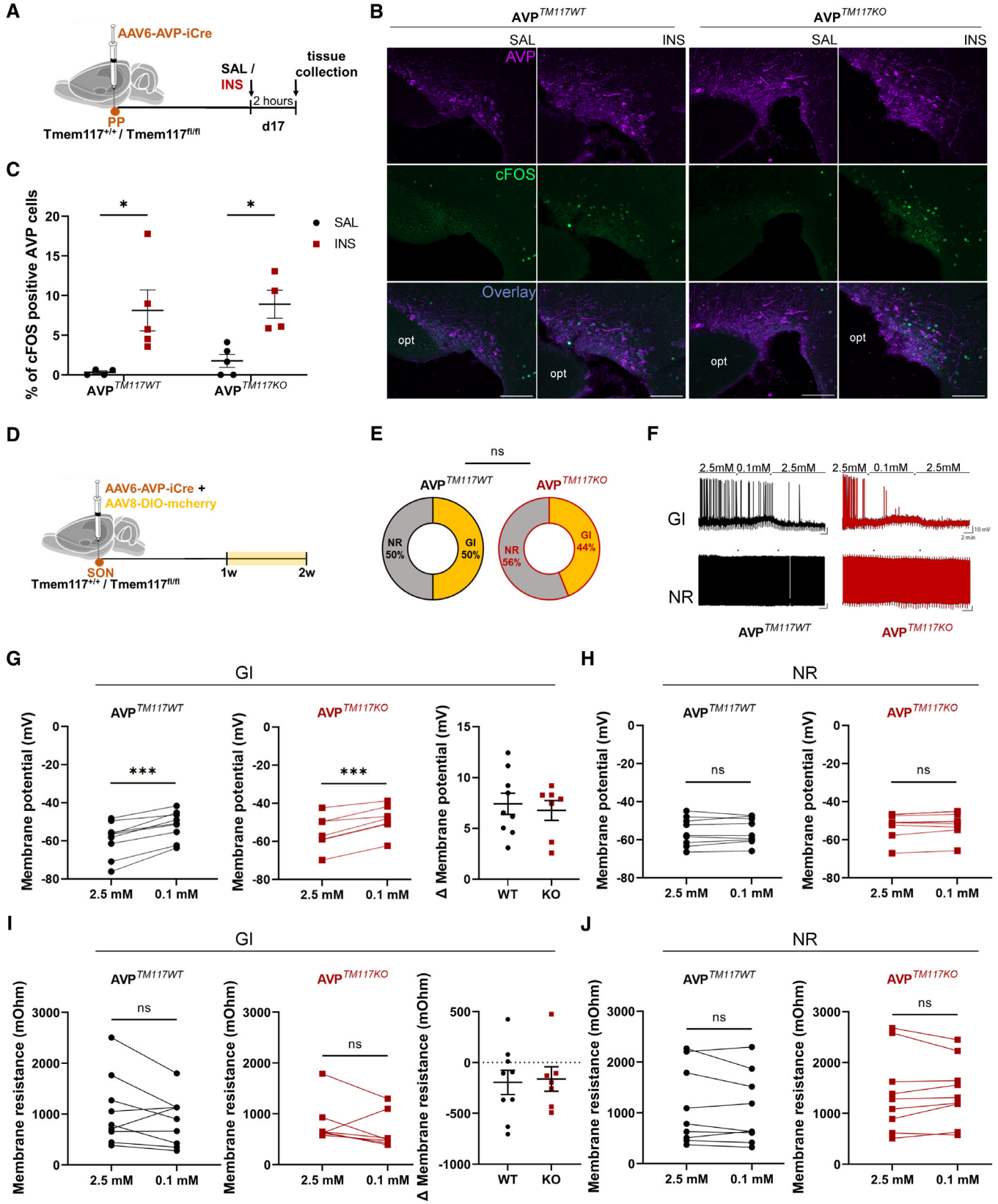

Figure 4.

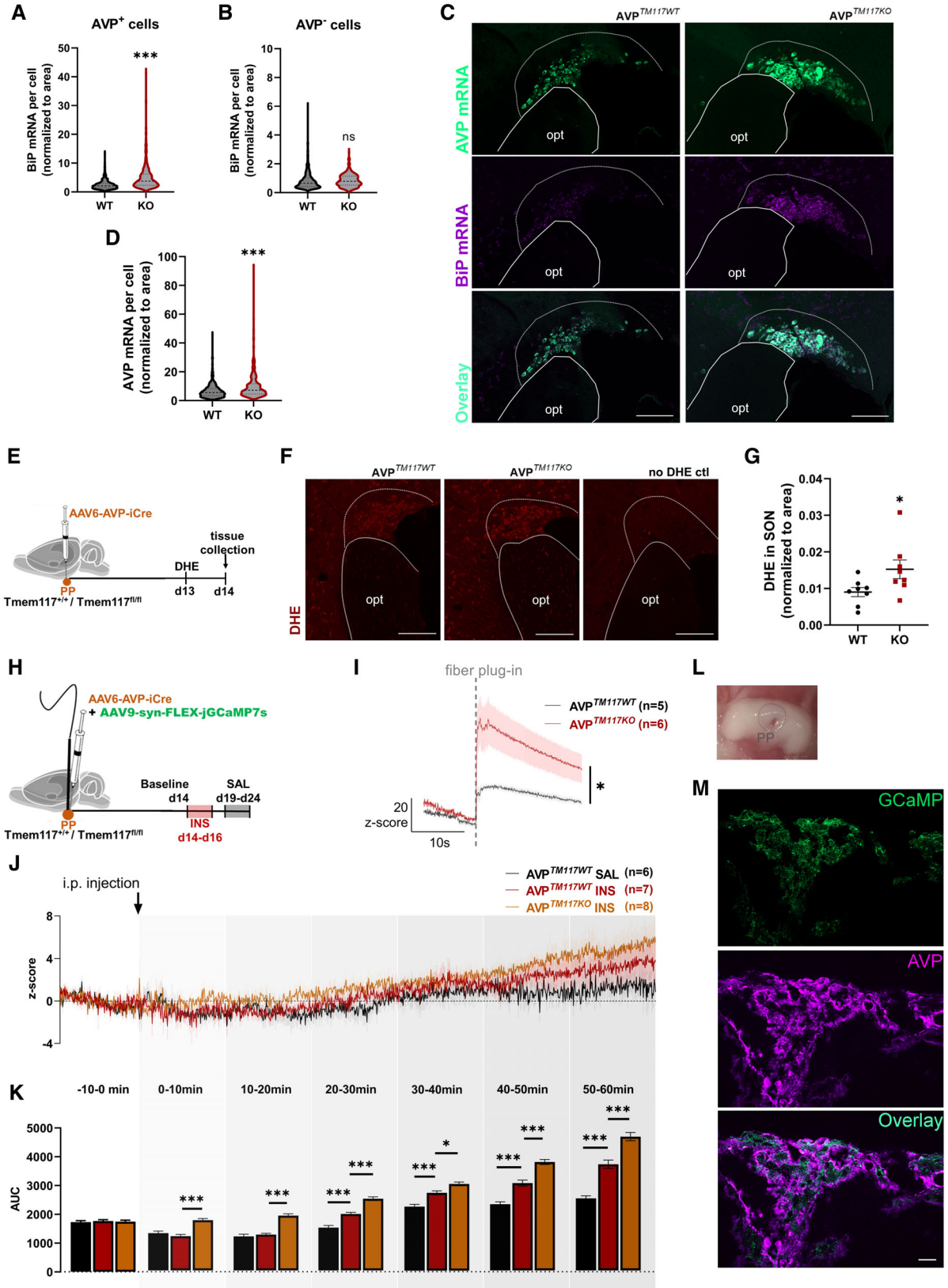
A
AVP+ cells
BiP mRNA per cell (normalized to area)
***
WT
KO
B
AVP- cells
ns
C
AVPTM117WT
AVPTM117KO
AVP mRNA
BiP mRNA
Overlay
opt
D
AVP mRNA per cell (normalized to area)
E
AAV6-AVP-iCre
tissue collection
DHE
PP
Tmem117+/+ / Tmem117fl/fl
d13
d14
F
no DHE ctl
DHE
G
DHE in SON (normalized to area)
H
+ AAV9-syn-FLEX-jGCaMP7s
Baseline d14
SAL d19-d24
INS d14-d16
I
fiber plug-in
AVPTM117WT (n=5)
AVPTM117KO (n=6)
20 z-score
10s
L
M
GCaMP
AVP
Overlay
J
i.p. injection
AVPTM117WT SAL (n=6)
AVPTM117WT INS (n=7)
AVPTM117KO INS (n=8)
z-score
K
-10-0 min
0-10min
10-20min
20-30min
30-40min
40-50min
50-60min
AUC

Figure 5.

Figure 5. *Tmem117* inactivation in AVP neurons increases AVP and BiP mRNA, ROS levels, and intracellular calcium *in vivo*.

A Quantification of BiP mRNA per cell in AVP-positive cells of the SON (n = 483–704 cells per group; each group consisted of four mice).
B Quantification of BiP mRNA per cell in AVP-negative cells of the SON (n = 347–584 cells per group; each group consisted of four mice).
C Fluorescence microscopy detection of AVP mRNA (green) and BiP mRNA (magenta) in the SON.
D Quantification of AVP mRNA per cell (n = 483–704 cells per group; each group consisted of four mice).
E Experimental scheme. AAV6-AVP-iCre was injected in the posterior pituitary of *Tmem117*$^{fl/fl}$ (AVP^{TM117KO}) or *Tmem117*$^{+/+}$ (AVP^{TM117WT}) mice. DHE was injected i.p. (50 mg/kg) 24 h before tissue collection.
F Fluorescence microscopy detection of DHE-derived fluorescence (red) in the SON.
G Quantification of DHE-derived fluorescence in the SON (n = 8 SON per group; each group consisted of four mice).
H Experimental scheme. AAV6-AVP-iCre was injected in the posterior pituitary of *Tmem117*$^{fl/fl}$ (AVP^{TM117KO}) or *Tmem117*$^{+/+}$ (AVP^{TM117WT}) mice. An optic fiber was implanted in the same area for signal analysis in freely moving mice.
I Basal calcium levels measured in AVP magnocellular terminals of AVP^{TM117WT} and AVP^{TM117KO} mice. The gray dashed line represents the time at which the optic fiber cable was plugged onto the implanted cannula (n = 5–6 mice per group).
J Calcium recordings in AVP magnocellular terminals 10 min before and 1 h after the i.p injection of insulin (red and orange) or saline (black). The vertical arrow corresponds to the i.p. injection (time = 0).
K Quantification of mean signal intensity in 10-min time bins (n = 6–8 mice per group).
L Stereoscope image of the pituitary gland depicting the optic fiber tract in the posterior pituitary.
M Fluorescence microscopy detection of GCaMP (green) in posterior pituitary. Immunofluorescent labeling was used to localize the AVP terminals (magenta).

Data information: AUC: area under the curve, AVP: vasopressin, d: day, DHE: dihydroethidium, INS: insulin, opt: optic tract, PP: posterior pituitary, SAL: saline, SON: supraoptic nucleus. Scale bar = 20 μm. For panels G and K, data are represented as mean ± SEM. For the violin plots of panels A–C, dashed lines correspond to the median value and dotted lines to the quartile values. A–C,G: unpaired t test; I: two-way ANOVA RM with Bonferroni *post hoc* test; K: one-way ANOVA with Tukey's *post hoc* test; *P < 0.05, ***P > 0.001.
Source data are available online for this figure.

of the Cre-infected AVP neurons had disappeared during the postinfection period. This was also reflected by a reduction in the total number of neurons in the SON, as measured by DAPI staining (Fig EV4E).

To determine whether the loss of AVP neurons would suppress the oversecretion phenotype, we injected AAV6-AVP-iCre in the posterior pituitary of *Tmem117*$^{fl/fl}$ (AVP^{TM117KO}) and *Tmem117*$^{+/+}$ (AVP^{TM117WT}) male mice and, except from the 2-week time point, we also assessed hormonal secretion upon insulin-induced hypoglycemia at the later time point of 1 month. Then, at the end of the experiment, brains were collected for histological analysis (Fig 6A). Immunofluorescence microscopy analysis revealed a significant reduction in the number of AVP neurons in the PVN and SON of *AVP*^{TM117KO} mice as compared to *AVP*^{TM117WT} mice (Fig 6B–D). Insulin-induced hypoglycemia reached the same level in both groups (Fig 6E), and induced a transiently enhanced secretion of CPP and GCG in AVP^{TM117KO} mice that was evident only at the early time point (Fig 6F and G). Correlation analysis between plasma CPP and GCG levels for each sample revealed a strong positive correlation (Fig 6H), further supporting their causal relationship. Thus, inactivation of *Tmem117* in AVP neurons led, over time, to cell death and the disappearance of the oversecretion phenotype.

Discussion

In this study, we characterized the site of expression and functional role of *Tmem117*, a genetically controlled, hypothalamic regulator of insulin-induced GCG secretion. We found that *Tmem117* is expressed in AVP magnocellular neurons and *Tmem117* inactivation increases hypoglycemia-induced CPP and GCG secretion. This phenotype is observed in male mice and only in the proestrus phase in female mice. c-Fos immunodetection showed that AVP neurons are activated by hypoglycemia and patch clamp analysis revealed that about half of them are GI neurons. Inactivation of *Tmem117* did not affect the glucose responsiveness of AVP neurons, but instead increased ER stress, elevated intracellular ROS, and Ca^{2+} concentrations, leading to increased AVP production and secretion. These results highlight the physiological role of AVP neurons in the control of GCG secretion and identify *Tmem117* as a novel regulator of their function.

Figure 6. *Tmem117* inactivation in AVP neurons over time triggers neuronal death.

A Experimental timeline. AAV6-AVP-iCre was injected in the posterior pituitary of *Tmem117*$^{fl/fl}$ (AVP^{TM117KO}) or *Tmem117*$^{+/+}$ (AVP^{TM117WT}) mice.
B Immunofluorescence microscopy detection of AVP in the PVN and the SON.
C Quantitation of AVP-positive cells in the PVN (n = 3–4 mice per group).
D Quantitation of AVP-positive cells in the SON (n = 3–4 mice per group).
E Glycemia 1 h after saline (black) or insulin (red) i.p. injections in AVP^{TM117WT} and AVP^{TM117KO} male mice (n = 8–9 mice per group).
F CPP plasma levels 1 h after saline or insulin injection in AVP^{TM117WT} and AVP^{TM117KO} male mice (n = 8 mice per group).
G GCG plasma levels 1 h after saline or insulin injection in AVP^{TM117WT} and AVP^{TM117KO} male mice (n = 8–9 mice per group).
H Correlation between the levels of plasma CPP and GCG in each sample (n = 24 samples per group; eight mice per group tested at three distinct time points).

Data information: 3V: third ventricle, AVP: vasopressin, d: day, INS: insulin, KO: AVP^{TM117KO}, SAL: saline, opt: optic tract, PVN: paraventricular nucleus, SON: supraoptic nucleus, WT: AVP^{TM117WT}. Scale bar = 100 μm. For panels C and D, lines correspond to the mean value per group and error bars represent ± SEM. For panels E–G, bars correspond to the mean value per group and error bars represent ± SEM. C,D: unpaired t test; E–G: two-way ANOVA for each time point in comparison to SAL baseline with Bonferroni *post hoc* test; *P < 0.05, **P < 0.01, ***P < 0.001.
Source data are available online for this figure.

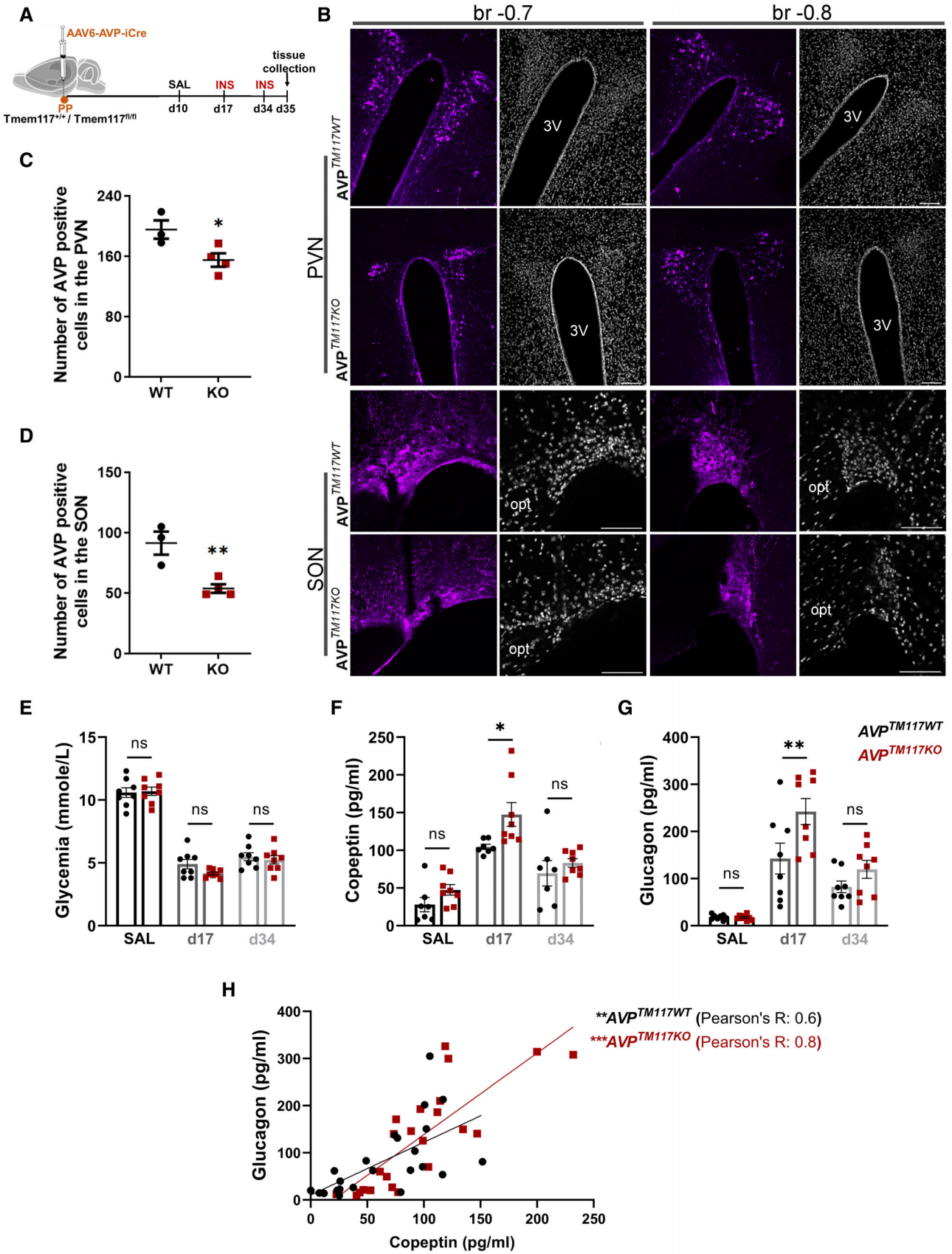
A
AAV6-AVP-iCre
tissue collection
SAL
INS
INS
PP
d10
d17
d34 d35
Tmem117+/+ / Tmem117fl/fl
B
br -0.7
br -0.8
PVN
SON
AVPTM117WT
AVPTM117KO
3V
opt
C
Number of AVP positive cells in the PVN
240
160
80
0
WT
KO
D
Number of AVP positive cells in the SON
150
100
50
0
WT
KO
E
Glycemia (mmole/L)
15
10
5
0
ns
SAL
d17
d34
F
Copeptin (pg/ml)
250
200
150
100
50
0
*
ns
G
Glucagon (pg/ml)
400
300
200
100
0
**
ns
AVPTM117WT
AVPTM117KO
H
Glucagon (pg/ml)
Copeptin (pg/ml)
0
50
100
150
200
250
**AVPTM117WT (Pearson's R: 0.6)
***AVPTM117KO (Pearson's R: 0.8)

Figure 6.

Tmem117 is an eight transmembrane domain-containing protein (Bürgi *et al*, 2016). We found it to be present in AVP neurons of the PVN and SON, with a widespread intracellular localization, from the soma to the axons and in their terminals located in the posterior pituitary, the site of AVP secretion in the bloodstream. The level of *Tmem117* mRNA expression in the hypothalamus of the BXD mouse lines used for the genetic screen showed strong and negative correlation with hypoglycemia-induced GCG secretion (Picard *et al*, 2022) (Fig EV1D). Our physiological studies indicated that AVP neurons are activated by insulin-induced hypoglycemia, leading to CPP secretion, a response that was augmented by *Tmem117* inactivation and was accompanied by increased GCG secretion. These observations are in agreement with previous studies showing increased secretion of AVP in response to hypoglycemia (Baylis & Robertson, 1980; Baylis *et al*, 1981; Chiodera *et al*, 1992) and that AVP stimulates GCG secretion through its binding to the AVP V1b receptor of pancreatic α cells (Dunning *et al*, 1984; Spruce *et al*, 1985; Gao *et al*, 1992; Yibchok-anun *et al*, 2004; Kim *et al*, 2021; Liu *et al*, 2021). On the other hand, these results are also in line with our genetic screen that showed a negative correlation between *Tmem117* expression and insulin-induced GCG secretion.

Interestingly, the effect of *Tmem117* inactivation on GCG secretion is sex dependent; it is present in male mice, but only during the proestrus phase in female mice. Circulating levels of estradiol peak during proestrus phase and have been linked to adaptations in AVP magnocellular neurons and their afferent connections (Sladek & Somponpun, 2008), as well as to decreased GCG secretion from pancreatic alpha cells (Godsland, 2005; Mårtensson *et al*, 2009). Thus, our data suggest a possible contribution of estradiol to the AVP-stimulated GCG release in conditions of hypoglycemia. Preceding studies have also reported that the CRR displays sex dimorphism (Steinbusch *et al*, 2016; Briski *et al*, 2017), though the precise mechanisms involved still need to be fully characterized. Given the complexity and redundancy of the CRR implicated pathways, this sex dimorphism is most probably a result of sex hormones acting at various sites and affecting different aspects of the response. Our data suggest that the action of estrogen on magnocellular AVP neurons is one of these aspects. AVP neurons express both nuclear and plasma membrane estrogen receptors that exert direct effects on intracellular signaling and AVP release (Sladek & Somponpun, 2008). Plasma concentration of AVP is decreased upon estradiol treatment in rodents (Peysner & Forsling, 1990) and during the follicular phase in women (Stachenfeld, 2008), suggesting a suppressing effect of estrogen on AVP secretion. Therefore, one could hypothesize that hypoglycemia-induced AVP secretion would be decreased during estradiol-rich phases of the estrus cycle. Our data appear in line with such a hypothesis, since plasma CPP levels during hypoglycemia tend to be lower in WT mice that are in the proestrus phase (Fig 2I, black dots, $P = 0.13$), but further studies focusing specifically on AVP secretion across the estrus cycle and its effect on CRR are required in order to get a detailed understanding of this interplay. What is clearly pointed out by our results is that inactivation of *Tmem117* in AVP neurons of female mice leads to increased AVP secretion during the estradiol-rich proestrus phase.

In order to investigate the mechanisms by which *Tmem117* inactivation regulates CPP secretion in hypoglycemic conditions, we explored the glucose responsiveness of the AVP neurons. First, c-Fos immunofluorescence analysis showed that insulin-induced hypoglycemia led to an approximately threefold increase in the activation of AVP neurons in the SON, suggesting that they are glucose responsive. This was confirmed by patch clamp analysis, which revealed that ~50% of them are GI neurons activated by low extracellular glucose concentrations. Thus, AVP neurons can respond to decreased glucose levels. Interestingly, a recent study reported that hypoglycemia can also activate AVP neurons through afferent connections arising from GI neurons of the basolateral medulla (Kim *et al*, 2021). Thus, AVP neurons are part of a brainstem hypothalamus neuronal circuit where hypoglycemia can be sensed by neurons located at multiple sites to activate the secretion of AVP leading to increased secretion of GCG.

Patch clamp and c-Fos immunofluorescence analysis revealed that inactivation of *Tmem117* does not affect the glucose responsiveness of AVP neurons. Instead, it induces ER stress and increases intracellular ROS and Ca^{2+} levels, leading to enhanced AVP production and secretion. These results extend previous observations made in the HCT116 cancer cells showing that *Tmem117* silencing increases ER stress and ROS production (Tamaki *et al*, 2017) and are in line with the reports that increased intracellular ROS stimulate AVP transcription in magnocellular neurons (St-Louis *et al*, 2012, 2014). It is striking that a small reduction in *Tmem117* expression in the SW480 cell line (~30%) led to a significantly increased expression of ER stress markers. This suggests that *Tmem117* expression level has an important regulatory role. This is compatible with the genetic screen that showed strong correlation across the BXD lines between the level of *Tmem117* expression and hypoglycemia-induced GCG secretion. Thus, fine-tuning of *Tmem117* expression appears as a physiological mean of controlling AVP neuron secretory capacity. This hypothesis is further supported by our data reporting decreased *Tmem117* mRNA levels in the SON in response to insulin-induced hypoglycemia. On the other hand, such a fine-tuning mechanism could also be implicated in pathological conditions, where a maladaptive upregulation of *Tmem117* expression would lead to decreased AVP secretion. In contrast, genetic inactivation of *Tmem117*, which leads to permanent increase in ER stress, ROS production, and elevated intracellular Ca^{2+} levels, is not compatible with the long-term survival of these neurons. Indeed, 1 month after induction of *Tmem117* recombination we observe neuronal death, probably as a result of apoptosis, as reported in the HCT116 cells with silencing of *Tmem117* (Tamaki *et al*, 2017).

Collectively, this study highlights the physiological role of the AVP neurons in the CRR and identifies *Tmem117* as a genetic determinant of AVP and GCG secretion. Inactivation of *Tmem117* did not affect the glucose-sensing properties of AVP GI neurons, but led to increased CPP secretion associated with increased ER stress, intracellular ROS, and Ca^{2+} levels, and increased AVP mRNA expression. Thus, Tmem117 emerges as a so far uncharacterized regulator of AVP neuron secretory capacity, by increasing AVP mRNA expression and secretion in response to hypoglycemia. Defining how Tmem117 controls these intracellular processes at the molecular level will, however, require future studies. Finally, this study further demonstrates that the central response to hypoglycemia is highly complex, integrating not only brainstem and hypothalamic glucose responsive neurons that activate the HPA axis and both branches of the autonomic nervous system, but also the secretion in the blood of AVP by magnocellular neurons.

Materials and Methods

Experimental models and subject details

Mice

All animal care and experimental procedures were in accordance with the Swiss National Institutional Guidelines of Animal Experimentation (OExA; 455.163) with license approval (VD3363, VD3674) issued by the Vétérinaire Cantonal (Vaud, Switzerland). Mice were housed up to five per cage in a temperature-controlled room with a 12-h light/dark cycle and ad libitum access to water and standard laboratory chow (SAFE 150). For all the experiments, 8- to 10-week-old mice were used.

Generation of Tmem117^{fl} mice

Tmem117^{fl} mice were generated by homologous recombination in embryonic stem cells (genOway, Lyon, France). A reporter cassette for targeting exon 3, preceded by a splice acceptor, was inserted in antisense into the respective intron. Both the cassette and the targeted exon were flanked by loxP sites and mutated loxP sites to enable deletion monitoring using the FLEx approach (Schnütgen *et al*, 2003) (Fig EV1A). The derived mouse line was developed onto a C57BL/6N background.

Tmem117^{fl};AVP-IRES2-Cre-D mice

Tmem117$^{fl/fl}$;AVP-IRES2-Cre-D$^{tg/+}$ mice were generated by crossing the *Tmem117*^{fl} line with the AVP-IRES2-Cre-D (Jackson Laboratory code: 023530) for verifying the specificity of the *Tmem117* antibody (Fig 1C and D).

Rosa26^{tdTomato} (Ai14) mice

Ai14 mice (Jackson Laboratory code: 007914) were used for verifying the specificity of the newly generated AAV6-AVP-iCre.

Cell lines

SW480 cells

The human colorectal cancer cell line SW480 (ATCC CCL-228) was cultured in Leibovitz's L-15 medium, supplemented with 10% fetal bovine serum (FBS). Cells were incubated at 37°C in a 0.3% CO_2 atmosphere and passaged twice per week up to 30 passages.

Method details

In vivo

Stereotaxic surgery/optic fiber cannula implantation

Mice were anesthetized with a ketamine and xylazine solution (100 mg/kg ketamine, 5 mg/kg xylazine injected i.p.) and were placed on a stereotaxic frame (Stoelting, Chicago, IL, USA). A small incision was made in the skin to reveal the skull. A small opening, to allow the passage of a 33-gauge needle, was made and the viral solution was injected at a rate of 100 nl/min. The stereotaxic coordinates (relative to the bregma) and total volume injected for each area were: posterior pituitary: AP: −3, ML: 0, DV: −5.8, 0° angle/400 nl; SON: AP: −0.46, ML: ±1.15, DV: −5.45, 0° angle/140 nl per hemisphere. After the viral injection, the incision was closed by suturing and an analgesic solution was provided (0.1 mg/kg buprenorphine s.c.). Ophthalmic ointment was used throughout the procedure to prevent eye dryness. A heat pad was used to maintain the proper body temperature.

For fiber photometry recordings, an optic fiber (Doric Lenses B280-2408-6.4) was implanted in the posterior pituitary after the viral injection and the incision was closed with dental cement.

For insulin-induced hypoglycemia experiments, 400 nL of AA6-AVP-iCre (8.1×10^{12} [viral genomes] vg/ml) were injected in the posterior pituitary. For electrophysiological recordings (Fig 4) and viability assessment (Fig EV4), 140 nl of a 1:1 mix of AAV6-AVP-iCre (8.1×10^{12} vg/ml) with AAV8-syn-DIO-mCherry (2.2×10^{13} vg/ml) or AAV9-syn-DIO-EGFP (2.4×10^{13} vg/ml) were injected per hemisphere in SON. For fiber photometry, 400 nl of a 1:1 mix of AAV6-AVP-iCre (8.1×10^{12} vg/ml) with AAV9-syn-FLEX-jGaMP7s (2.5×10^{13} vg/ml) were injected in the posterior pituitary.

Insulin-induced hypoglycemia; blood collection

Mice were food deprived for 6 h (8 am–2 pm). At 12 pm, they were placed in individual cages and glycemia was measured. At 1 pm, glycemia was measured again and the mice were injected i.p. with either saline (baseline control) or insulin (0.8 U/kg). At 2 pm, glycemia was measured again and 100-120 µl of blood were collected under isoflurane-induced general anesthesia by submandibular vein incision.

Fiber photometry

Starting 5 days after surgery, mice were habituated to the recording cage and placement of the optic fiber in 30-min sessions at least twice per week for 2 weeks. On the day of recording, the mice were placed in the recording cage for 30 min and signal recording was started. The optic fiber was then connected to capture the baseline and stimulated signal intensity. The fiber photometry system was from Doric Lenses using LED light sources for GCaMP (465 nm) and isosbestic (405 nm) measurements; signal was recorded and analyzed using the Doric Neuroscience Studio software. The GCaMP7 signal was first normalized over the isosbestic signal ($i = i_{465} - i_{405}$) and then over the mean signal for the whole trace ($\Delta F/F0$). Each point was then normalized to the baseline signal to obtain the corresponding z score calculated using the formula: $z_{(i)} = [\Delta F/F0_{(i)} - \text{median}\ (\Delta F/F0_{\ \text{baseline}})/\text{MAD}_{\text{baseline}}]$. For baseline intensity traces, z-score generation was calculated based on a 1-s recording period before the cable was plugged onto the optic cannula. For insulin-induced hypoglycemia traces, z-score generation was calculated based on the baseline signal recorded over 10 min before the i.p. injection.

Estrus cycle monitoring

The estrus cycle phase was identified based on vaginal cytology samples after violet crystal staining (McLean *et al*, 2012).

Tissue collection

For immunofluorescence microscopy analysis, mice were transcardially perfused with 10 ml ice-cold phosphate-buffered saline (PBS: 137 mM NaCl, 2.7 mM KCl, 10 mM Na_2HPO_4, 1.8 mM KH_2PO_4) followed by 40 ml ice-cold paraformaldehyde (PFA, 4%) in PBS. Brain and pituitary were postfixed in 4% PFA O/N at 4°C and then kept for 24 h in 30% sucrose in PBS at 4°C. Tissues were frozen and stored at −80°C.

For SON and PVN DNA extraction, fresh brains were collected and kept in RNAlater solution (Thermo Fisher Scientific) at 4°C for 1 week. Then, 250-µm-thick vibratome sections were prepared and

PVN and SON nuclei were dissected under a stereomicroscope. Microdissected tissue was frozen with dry ice and stored at −80°C, before DNA extraction.

Ex vivo

Electrophysiological recordings

Tmem117$^{fl/fl}$ and *Tmem117*$^{+/+}$ mice were injected in the SON with an AAV6-AVP-iCre and an AAV8-DIO-mCherry. One to two weeks later, they were deeply anesthetized with isoflurane, decapitated, and their brain taken out and immediately placed in an ice-cold high-glucose artificial cerebrospinal fluid (ACSF) containing (in mM): 125 NaCl, 2.5 KCl, 1.25 NaH_2PO_4, 1 $MgCl_2$, 2 $CaCl_2$, 26 $NaHCO_3$, and 10 glucose (300 ± 5 mOsm) equilibrated with 95% O_2/5% CO_2. Coronal sections (250 μm) containing SON were prepared using a vibratome (VT1000S, Leica) and immediately transferred to an oxygenated ACSF solution containing 2.5 mM glucose and maintained at 32°C for at least 1 h before starting the recordings. Experiments were performed using an upright epifluorescence microscope (BX51WI, Olympus, Japan) mounted on a motorized stage coupled to a micromanipulator (MPC-325, Sutter Instrument, USA) and equipped with a mercury lamp and an Evolve EMCCD camera (Teledyne Photometrics Technology, USA) and appropriate filters allowing the visualization of mCherry-expressing neurons.

Glucose responsiveness of AVP neurons was then assessed in the whole-cell configuration using a MultiClamp 700B amplifier associated with a 1440A Digidata digitizer (Molecular Devices). Borosilicate glass pipettes (resistance: 2–5 MΩ.; GC150F-7.5, Harvard Apparatus, USA) were prepared with a P-97 horizontal micropipette puller (Sutter Instrument, USA). The patch pipettes were filled with an intrapipette solution containing (in mM): 130 K-gluconate, 5 NaCl, 1 $MgCl_2$, 10 NaPhosphocreatinine, 10 HEPES, 0.2 EGTA, 4 MgATP, 0.5 Na_2GTP (pH 7.2–7.4; 280 ± 5 mOsm). Membrane potential and membrane resistance were monitored in current-clamp mode in the presence of 2.5 mM or 0.1 mM glucose after a 10- to 15-min baseline. Neurons with an access resistance > 25 MΩ or changing by > 20% during the recording were excluded from the analysis. Signals were filtered at 2 kHz, digitized at 10 kHz, and collected online with a pClamp 10 data acquisition system (Molecular Devices).

Cell culture

SW480 cells were plated in six-well tissue culture plate at a density of 300,000 cells/well. After 48 h cells were transfected with siRNA against *Tmem117* or siRNA control (30 pmol/well) with lipofectamine RNAiMAX (Thermo Fisher Scientific, Cat# 13778100). Forty-eight hours after transfection, cells were trypsinized and pelleted by mild centrifugation (300 *g* for 3 min). Supernatant was removed and cell pellet was used for RNA and protein extraction using Qiagen RNeasy Mini kit.

Sample preparation/analysis

Immunofluorescence microscopy

Tissue sections (25-μm thick) were washed with PBS for 5 min at RT, incubated with blocking solution (2% normal goat serum +0.3% Triton X-100 in PBS) for 1 h at RT and then incubated O/N with primary antibodies (Guinea Pig anti-(Arg8)-Vasopressin, BMA Biomedicals, Cat# T-5048; Rabbit anti-Tmem117, Novus, Cat# NBP1-94078) in blocking solution at 4°C. Next, sections were washed with PBS 3 times for 10 min, incubated with secondary antibodies (Goat anti-Rabbit Alexa Fluor 488, Molecular Probes, Cat# A-11078; Goat anti-Guinea pig Cy5, Abcam, Cat# ab102372) in blocking solution for 2 h at RT, washed again with PBS 3 times for 10 min, incubated with DAPI (1:10,000 in PBS) for 20 min at RT, washed with PBS 3 times for 10 min, allowed to dry, and finally mounted using fluoromount (Sigma F4680).

For c-Fos immunodetection tissue sections were washed with PBS for 5 min at RT, incubated with blocking solution (4% normal goat serum +0.3% Triton X-100 in PBS) for 1 h at RT and then incubated O/N with primary antibody for c-Fos (Rabbit anti-cFos, Cell Signaling, Cat# 2250) in blocking solution at RT. Next, sections were washed with PBS 3 times for 10 min, incubated with secondary antibody in blocking solution for 3 h at RT, washed again with PBS 3 times for 10 min, and incubated O/N with primary antibody for AVP in blocking solution at 4°C. Next, sections were washed with PBS 3 times for 10 min, incubated with secondary antibody in blocking solution for 3 h at RT, washed again with PBS 3 times for 10 min, incubated with DAPI (1:10,000 in PBS) for 20 min at RT, washed with PBS 3 times for 10 min, allowed to dry, and finally mounted using fluoromount.

For all secondary antibodies the final concentration in the working solution was 1:500. For primary antibodies the concentrations used were: anti-Tmem117 1:250, anti-AVP 1:250, anti-cFos 1:1,000.

In situ *hybridization (RNAscope)*

Tissue sections (25-μm thick) containing the SON were costained by *in situ* hybridization for AVP mRNA (Cat# 401391) and BiP mRNA (Cat# 438831-C3) using RNAscope probes and RNAscope Fluorescent Multiplex Detection Reagents (Advanced Cell Diagnostics, Newark, CA, USA) following manufacturer's instructions.

DHE fluorescent labeling

Tissue sections were washed with PBS for 5 min at RT, allowed to dry, and mounted using fluoromount (Sigma F4680).

Quantitative microscopy analysis

Fluorescence images were acquired on a ZEISS Axio Imager.M2 microscope, equipped with ApoTome.2, and a Camera Axiocam 702 mono (Zeiss, Germany). Specific filter cubes were used for the visualization of green (Filter set 38 HE eGFP shift free (E) EX BP 470/40, BS FT 495, EM BP 525/50), red (Filter set 43 HE Cy 3 shift free (E) EX BP 550/25, BS FT 570, EM BP 605/70), blue (Filter set 49 DAPI shift free (E) EX G 365, BS FT 395, EM BP 445/50) fluorescence, and far red (Filter set 50 Cy 5 shift free [E] EX BP 640/30, BS FT 660, EM BP 690/50). Different magnifications were selected using a Zeiss 20x objective (Objective Plan-Apochromat 20x/0.8 M27, FWD = 0.55 mm) and a 40x oil-immersion objective (Objective C Plan-Apochromat 40x/1.4 Oil DIC M27 [FWD = 0.13 mm]). For super-resolution microscopy the ZEISS ELYRA7 SIM^2 system was used with an 63x oil-immersion objective.

Cell quantification in PVN and SON was performed on images derived from two consecutive hypothalamic sections for each mouse (bregma −0.7 and −0.8). Fluorescence intensity quantification was performed using the QuPath-0.3.2 software on images derived from two consecutive hypothalamic sections for each mouse (bregma −0.7 and −0.8). Neuroanatomical landmarks (third ventricle, optic

tract, fornix) and DAPI staining were used to define the region of interest and cell area was marked manually by a blinded experimenter.

Western blot

The protein content of the samples was quantified by Bradford assay. Total protein (25 μg) per sample were prepared in SDS-PAGE sample buffer (2% SDS, 10% glycerol, 50 mM Tris, 0.1% bromophenol blue, 5% β-mercaptoethanol) and separated on a 10% SDS-PAGE gel. Proteins were transferred onto a nitrocellulose membrane, incubated with blocking solution (3% milk in PBS-T [PBS + 0.1% Tween-20]) for 1 h at RT, washed with PBS-T 3 times for 10 min, and incubated O/N at 4°C with primary antibody (Rabbit anti-Calnexin, Abcam, Cat# ab133615) at a dilution of 1:1,000 in PBS-T. Then membranes were washed with PBS-T 3 times for 10 min, incubated for 1 h at RT with horseradish peroxidase (HRP)-conjugated secondary antibody (Anti-Rabbit HRP, Amersham, Cat# NA934) at a dilution of 1:10,000 in blocking solution, washed again with PBS-T 3 times for 10 min, incubated for 1 min with enhanced chemiluminescence (ECL, Amersham) buffer, and the HRP-mediated chemiluminescence signal was detected/imaged using the Fusion FX6 Spectra imaging platform (VILBER). The derived images were analyzed for band intensity using ImageJ. The calnexin signal of each sample was normalized to the total protein (Pierce Reversible Protein Stain Kit). Data are presented as percent of the control.

DNA extraction/PCR

DNA was extracted from microdissected tissue using the Arcturus Picopure DNA extraction kit (Applied Biosystems, Ref # KIT0103). The extracted DNA was then subjected to PCR for detection of recombination using the following primers: 5′-CTTTCTTCAT AAAAAGCCGGAAGGCATTAC-3′ (212), 5′-GCCTGAAATATAAAT ATCGCAAGTGAGTGTGC-3′ (213), 5’-CAACTGACCTTGGGCAAGAA CATAAAGTG-3′ (216) (graphical representation Fig EV1A).

RNA extraction/real-time PCR

Total RNA was extracted from SW480 cell pellets using the Qiagen RNeasy Mini kit based on manufacturer’s instructions and from microdissected tissue using the Arcturus Picopure RNA extraction kit (Applied Biosystems, Ref # KIT0204). RNA was then reverse transcribed, and the derived cDNA was quantified using specific primers against *Tmem117* (FW:5′-TGTGATGCAGGACTGGGAAT-3′; RV:5′-TTGAACTGCATGTGAGGCGT-3′), *Xbp1* (FW:5′-TGGCCGGGT CTGCTGAGTCCG-3′; RV:5′-ATCCATGGGGAGATGTTCTGG-3′), *us Xbp1* (FW:5′-CAGCACTCAGACTACGTGCA-3′; RV:5′-ATCCATGGG-GAGATGTTCTGG-3′), *sXbp1* (FW:5′-CTGAGTCCGAATCAGGTGC AG-3′; RV:5′-ATCCATGGGGAGATGTTCTGG-3′), *BiP* (FW:5′-TGTTC AACCAATTATCAGCAAACTC-3′; RV:5′-TAGGTGGTCCCCAAGTC GAT-3′). Expression data were normalized to the housekeeping gene *Gusb* (FW: 5′-CCACCAGGGACCATCCAAT-3′; RV: 5′-AGTCAAAAT ATGTGTTCTGGACAAAGTAA-3′).

Quantification of circulating hormones

CPP and GCG levels in the plasma were quantified by Copeptin ELISA (MyBioSource, Cat# MBS2020621) and Glucagon ELISA (Mercodia, Cat# 10-1281-01), respectively, based on the manufacturer’s instructions.

Constructs/cloning/AAV packaging

The p2.0VPI.iCre (AVP-iCre) plasmid was generated by subcloning the iCre sequence (AgeI 2732nt, NotI 3813nt) from pCDH-CB-iCre plasmid (Addgene # 72257) in the p2.0VPI.EGFP backbone (AgeI 6237nt, NotI 6972nt; Addgene # 40868) (see Fig EV1). The packaging of the plasmid in the AAV6 was performed by the University of North Carolina (Chapel Hill, NC) vector core.

The TM117-GFP plasmid was provided by the Van der Goot group (EPFL, Lausanne; Bürgi *et al*, 2016).

eQTL analysis

eQTL mapping was performed using the R package R/qtl (Broman *et al*, 2003) with a genotype map from the BXD panel composed of GeneNetwork genotypes (www.genenetwork.org) merged with available RNA sequencing data from whole hypothalamic tissue (Picard *et al*, 2016). eQTL interval mapping was calculated using the expected maximization algorithm, a 5% genotyping error rate, and pseudomarkers were generated every cM. eQTL location was obtained by 6.915 likelihood ratio statistics (LRS) support intervals. Significant eQTLs were determined for the trait using a 5% false discovery rate threshold estimated from 1,000 permutations.

Quantification and statistical analysis

All graphs and statistical analysis were generated using Prism software (GraphPad Prism 9), further details regarding sample size and the statistical analysis used in each case can be found in the corresponding figure legends. In brief, for experiments concerning comparisons between two groups on a single independent variable (Figs 2H–J, 3C, F, H, and I, 4GΔ and IΔ, 5A, B, D, and G, 6C and D, EV3A–D, and EV4D), we used unpaired two-tailed *t* test. For experiments concerning comparisons between two dependent measurements (Fig 4G–J), we used paired two-tailed *t* test. For those concerning comparisons among three groups on a single independent variable (Figs 5K and EV4C and E), we used one-way ANOVA with Tukey’s *post hoc* test. For two-factor designs concerning repeated measures (Figs 2B–G, 5I and 6E–G), we used two-way ANOVA RM with Bonferroni *post hoc* test. For two-factor designs concerning nonrepeated measures (Fig 4C), we used two-way ANOVA with Tukey’s *post hoc* test. For the comparison of neuronal subpopulation proportion (Fig 4E), we used Fisher’s exact test. In all graphs, error bars are depicting ± SEM.

Data availability

No primary datasets have been generated and deposited.

Expanded View for this article is available online.

Acknowledgments

We thank Wanda Dolci for the excellent technical support, Prof. G Van der Goot for kindly providing the TM117-GFP plasmid, and ZEISS and the EPFL Bioimaging and Optics Platform for the access to the ELYRA7 SIM^2 super-resolution microscopy apparatus. This work was supported by a European Research Council Advanced Grant (Integrate, No. 694798) and a Swiss National Science Foundation grant (310030-182496) to BT, and has received funding from the Innovative Medicines Initiative 2 Joint Undertaking (JU) under grant

agreement No. 777460 (HypoRESOLVE). The JU receives support from the European Union's Horizon 2020 research and innovation program and EFPIA and T1D Exchange, JDRF, International Diabetes Federation (IDF), The Leona M. and Harry B. Helmsley Charitable Trust. Open access funding provided by Universite de Lausanne.

Author contributions

Sevasti Gaspari: Conceptualization; formal analysis; investigation; visualization; methodology; writing – original draft; project administration; writing – review and editing. **Gwenaël Labouèbe:** Formal analysis; investigation; visualization; methodology; writing – review and editing. **Alexandre Picard:** Formal analysis; writing – review and editing. **Xavier Berney:** Formal analysis; methodology. **Ana Rodriguez Sanchez-Archidona:** Software; visualization; writing – review and editing. **Bernard Thorens:** Conceptualization; resources; supervision; funding acquisition; visualization; writing – original draft; project administration; writing – review and editing.

Disclosure and competing interests statement

The authors declare that they have no conflict of interest.

References

Baylis PH, Robertson GL (1980) Rat vasopressin response to insulin-induced hypoglycemia. *Endocrinology* 107: 1975 – 1979

Baylis PH, Zerbe RL, Robertson GL (1981) Arginine vasopressin response to insulin-induced hypoglycemia in man. *J Clin Endocrinol Metab* 53: 935 – 940

Beall C, Ashford ML, McCrimmon RJ (2012) The physiology and pathophysiology of the neural control of the counterregulatory response. *Am J Physiol Regul Integr Comp Physiol* 302: R215 – R223

Bisgaard Bengtsen M, Møller N (2021) Mini-review: glucagon responses in type 1 diabetes – a matter of complexity. *Physiol Rep* 9: e15009

Briski KP, Alhamami HN, Alshamrani A, Mandal SK, Shakya M, Ibrahim MHH (2017) Sex differences and role of estradiol in hypoglycemia-associated counter-regulation. In *Sex and Gender Factors Affecting Metabolic Homeostasis, Diabetes and Obesity*, Mauvais-Jarvis F (ed), pp 359 – 383. Cham: Springer International Publishing

Broman KW, Wu H, Sen Ś, Churchill GA (2003) R/QTL: QTL mapping in experimental crosses. *Bioinformatics* 19: 889 – 890

Bürgi J, Xue B, Uversky VN, van der Goot FG (2016) Intrinsic disorder in transmembrane proteins: roles in signaling and topology prediction. *PLoS One* 11: e0158594

Cheng AH, Fung SW, Cheng H-YM (2019) Limitations of the Avp-IRES2-Cre (JAX #023530) and Vip-IRES-Cre (JAX #010908) models for chronobiological investigations. *J Biol Rhythms* 34: 634 – 644

Chiodera P, Volpi R, Capretti L, Speroni G, Marcato A, Rossi G, Coiro V (1992) Hypoglycemia-induced arginine vasopressin and oxytocin release is mediated by glucoreceptors located inside the blood-brain barrier. *Neuroendocrinology* 55: 655 – 659

Cryer PE (2012) Minireview: glucagon in the pathogenesis of hypoglycemia and hyperglycemia in diabetes. *Endocrinology* 153: 1039 – 1048

Dunning BE, Moltz JH, Fawcett CP (1984) Modulation of insulin and glucagon secretion from the perfused rat pancreas by the neurohypophysial hormones and by desamino-D-arginine vasopressin (DDAVP). *Peptides* 5: 871 – 875

Gaisano H, MacDonald P, Vranic M (2012) Glucagon secretion and signaling in the development of diabetes. *Front Physiol* 3: 349

Gao ZY, Gérard M, Henquin JC (1992) Glucose- and concentration-dependence of vasopressin-induced hormone release by mouse pancreatic islets. *Regul Pept* 38: 89 – 98

Garfield AS, Shah BP, Madara JC, Burke LK, Patterson CM, Flak J, Neve RL, Evans ML, Lowell BB, Myers MG *et al* (2014) A parabrachial-hypothalamic cholecystokinin neurocircuit controls counterregulatory responses to hypoglycemia. *Cell Metab* 20: 1030 – 1037

Giorgi C, Danese A, Missiroli S, Patergnani S, Pinton P (2018) Calcium dynamics as a machine for decoding signals. *Trends Cell Biol* 28: 258 – 273

Godsland IF (2005) Oestrogens and insulin secretion. *Diabetologia* 48: 2213 – 2220

Iurlaro R, Muñoz-Pinedo C (2016) Cell death induced by endoplasmic reticulum stress. *FEBS J* 283: 2640 – 2652

Jumper J, Evans R, Pritzel A, Green T, Figurnov M, Ronneberger O, Tunyasuvunakool K, Bates R, Žídek A, Potapenko A *et al* (2021) Highly accurate protein structure prediction with AlphaFold. *Nature* 596: 583 – 589

Kim A, Knudsen JG, Madara JC, Benrick A, Hill T, Abdul-Kadir L, Kellard JA, Mellander L, Miranda C, Lin H *et al* (2021) Arginine-vasopressin mediates counter-regulatory glucagon release and is diminished in type 1 diabetes. *Elife* 10: e72919

Labouèbe G, Thorens B, Lamy C (2018) GLUT2-expressing neurons as glucose sensors in the brain: electrophysiological analysis. *Methods Mol Biol* 1713: 255 – 267

Lamy CM, Sanno H, Labouèbe G, Picard A, Magnan C, Chatton J-Y, Thorens B (2014) Hypoglycemia-activated GLUT2 neurons of the nucleus tractus solitarius stimulate vagal activity and glucagon secretion. *Cell Metab* 19: 527 – 538

Liu L, Dattaroy D, Simpson KF, Barella LF, Cui Y, Xiong Y, Jin J, König GM, Kostenis E, Roman JC *et al* (2021) Gq signaling in α cells is critical for maintaining euglycemia. *JCI Insight* 6: e152852

Mårtensson UEA, Salehi SA, Windahl S, Gomez MF, Swärd K, Daszkiewicz-Nilsson J, Wendt A, Andersson N, Hellstrand P, Grände P-O *et al* (2009) Deletion of the G protein-coupled receptor 30 impairs glucose tolerance, reduces bone growth, increases blood pressure, and eliminates estradiol-stimulated insulin release in female mice. *Endocrinology* 150: 687 – 698

Marty N, Dallaporta M, Thorens B (2007) Brain glucose sensing, counterregulation, and energy homeostasis. *Physiology (Bethesda)* 22: 241 – 251

McLean AC, Valenzuela N, Fai S, Bennett SAL (2012) Performing vaginal lavage, crystal violet staining, and vaginal cytological evaluation for mouse estrous cycle staging identification. *J Vis Exp* 67: e4389

Meek TH, Nelson JT, Matsen ME, Dorfman MD, Guyenet SJ, Damian V, Allison MB, Scarlett JM, Nguyen HT, Thaler JP *et al* (2016) Functional identification of a neurocircuit regulating blood glucose. *Proc Natl Acad Sci U S A* 113: E2073 – E2082

Peirce JL, Lu L, Gu J, Silver LM, Williams RW (2004) A new set of BXD recombinant inbred lines from advanced intercross populations in mice. *BMC Genet* 5: 7

Peysner K, Forsling ML (1990) Effect of ovariectomy and treatment with ovarian steroids on vasopressin release and fluid balance in the rat. *J Endocrinol* 124: 277 – 284

Picard A, Soyer J, Berney X, Tarussio D, Quenneville S, Jan M, Grouzmann E, Burdet F, Ibberson M, Thorens B (2016) A genetic screen identifies hypothalamic Fgf15 as a regulator of glucagon secretion. *Cell Rep* 17: 1795 – 1806

Picard A, Metref S, Tarussio D, Dolci W, Berney X, Croizier S, Labouebe G, Thorens B (2021) Fgf15 neurons of the dorsomedial hypothalamus control glucagon secretion and hepatic gluconeogenesis. *Diabetes* 70: 1443 – 1457

Picard A, Berney X, Castillo-Armengol J, Tarussio D, Jan M, Sanchez-Archidona AR, Croizier S, Thorens B (2022) Hypothalamic Irak4 is a genetically controlled regulator of hypoglycemia-induced glucagon secretion. *Mol Metab* 61: 101479

Ponzio TA, Fields RL, Rashid OM, Salinas YD, Lubelski D, Gainer H (2012) Cell-type specific expression of the vasopressin gene analyzed by AAV mediated gene delivery of promoter deletion constructs into the rat SON in vivo. *PLoS One* 7: e48860

Ramnanan CJ, Edgerton DS, Kraft G, Cherrington AD (2011) Physiologic action of glucagon on liver glucose metabolism. *Diabetes Obes Metab* 13: 118 – 125

Salegio EA, Samaranch L, Kells AP, Mittermeyer G, San Sebastian W, Zhou S, Beyer J, Forsayeth J, Bankiewicz KS (2013) Axonal transport of adeno-associated viral vectors is serotype-dependent. *Gene Ther* 20: 348 – 352

Schnütgen F, Doerflinger N, Calléja C, Wendling O, Chambon P, Ghyselinck NB (2003) A directional strategy for monitoring Cre-mediated recombination at the cellular level in the mouse. *Nat Biotechnol* 21: 562 – 565

Siafarikas A, Johnston RJ, Bulsara MK, O'Leary P, Jones TW, Davis EA (2012) Early loss of the glucagon response to hypoglycemia in adolescents with type 1 diabetes. *Diabetes Care* 35: 1757 – 1762

Sladek CD, Somponpun SJ (2008) Estrogen receptors: their roles in regulation of vasopressin release for maintenance of fluid and electrolyte homeostasis. *Front Neuroendocrinol* 29: 114 – 127

Spruce BA, McCulloch AJ, Burd J, Orskov H, Heaton A, Baylis PH, Alberti KG (1985) The effect of vasopressin infusion on glucose metabolism in man. *Clin Endocrinol (Oxf)* 22: 463 – 468

Stachenfeld NS (2008) Sex hormone effects on body fluid regulation. *Exerc Sport Sci Rev* 36: 152 – 159

Stanley SA, Kelly L, Latcha KN, Schmidt SF, Yu X, Nectow AR, Sauer J, Dyke JP, Dordick JS, Friedman JM (2016) Bidirectional electromagnetic control of the hypothalamus regulates feeding and metabolism. *Nature* 531: 647 – 650

Stanley S, Moheet A, Seaquist ER (2019) Central mechanisms of glucose sensing and Counterregulation in defense of hypoglycemia. *Endocr Rev* 40: 768 – 788

Steinbusch LKM, Picard A, Bonnet MS, Basco D, Labouèbe G, Thorens B (2016) Sex-specific control of fat mass and Counterregulation by hypothalamic glucokinase. *Diabetes* 65: 2920 – 2931

St-Louis R, Parmentier C, Raison D, Grange-Messent V, Hardin-Pouzet H (2012) Reactive oxygen species are required for the hypothalamic osmoregulatory response. *Endocrinology* 153: 1317 – 1329

St-Louis R, Parmentier C, Grange-Messent V, Mhaouty-Kodja S, Hardin-Pouzet H (2014) Reactive oxygen species are physiological mediators of the noradrenergic signaling pathway in the mouse supraoptic nucleus. *Free Radic Biol Med* 71: 231 – 239

Strembitska A, Labouèbe G, Picard A, Berney XP, Tarussio D, Jan M, Thorens B (2022) Lipid biosynthesis enzyme Agpat5 in AgRP-neurons is required for insulin-induced hypoglycemia sensing and glucagon secretion. *Nat Commun* 13: 5761

Tamaki T, Kamatsuka K, Sato T, Morooka S, Otsuka K, Hattori M, Sugiyama T (2017) A novel transmembrane protein defines the endoplasmic reticulum stress-induced cell death pathway. *Biochem Biophys Res Commun* 486: 149 – 155

Tesfaye N, Seaquist ER (2010) Neuroendocrine responses to hypoglycemia. *Ann N Y Acad Sci* 1212: 12 – 28

Thorens B (2022) Neuronal regulation of glucagon secretion and gluconeogenesis. *J Diabetes Investig* 13: 599 – 607

Varadi M, Anyango S, Deshpande M, Nair S, Natassia C, Yordanova G, Yuan D, Stroe O, Wood G, Laydon A *et al* (2022) AlphaFold protein structure database: massively expanding the structural coverage of protein-sequence space with high-accuracy models. *Nucleic Acids Res* 50: D439 – D444

Yibchok-anun S, Abu-Basha EA, Yao C-Y, Panichkriangkrai W, Hsu WH (2004) The role of arginine vasopressin in diabetes-associated increase in glucagon secretion. *Regul Pept* 122: 157 – 162

Zhivotovsky B, Orrenius S (2011) Calcium and cell death mechanisms: a perspective from the cell death community. *Cell Calcium* 50: 211 – 221